Adaptive aberration correction of GRIN lenses for confocal endomicroscopy

W. M. Lee and S. H. Yun*

Harvard Medical School and Wellman Center for Photomedicine, Massachusetts General Hospital, 40 Blossom Street, Boston, Massachusetts 02114, USA

**Corresponding author: syun@hms.harvard.edu*

Received August 11, 2011; revised October 17, 2011; accepted October 20, 2011; posted October 21, 2011 (Doc. ID 152748); published November 28, 2011

Graded-index (GRIN) lenses serve as a key component for miniature endoscopes because of their small diameters and ease of assembly. However, the nonaplanatic nature of GRIN lenses causes inherent spatial aberrations that lower image resolution and sharpness. Here we present the diagnosis of the aberrations in GRIN probes and the use of adaptive optics to compensate for the wavefront errors in the endoscope. Two different operation schemes based on preset and *in situ* measurements are demonstrated, both resulting in a substantial reduction of the wavefront error from 0.42 to <0.1 μm. © 2011 Optical Society of America

OCIS codes: 010.1080, 220.1000, 170.2150.

Endoscopic fluorescence microscopy has emerged as a powerful tool for the visualization of cellular processes *in vivo* in internal organs [1–3]. However, the fabrication of miniature compound objectives for small-diameter endoscopes remains a challenge. An attractive alternative to compound objective lenses is a microendoscope based on GRIN rod lenses [2–4]. GRIN endoscopes offer several advantages, including low cost, small diameters (<1 mm), long lengths, and relatively high NA (NA = 0.4 – 0.6), that are appropriate for minimally invasive imaging of internal tissues with single-cell resolution [2–4]. However, compared to diffraction-limited objectives of the equivalent NA, most GRIN endoscopes have been operating with lower resolution and image contrast due to optical aberrations. Several factors contribute to the aberrations. A typical GRIN lens has a parabolic refractive index distribution decreasing from the central axis to the circumference along the radius [5]. The parabolic profile inherently possesses spherical and other types of aberration, and their magnitudes increase with the length and NA of the GRIN lens. Some types of the aberration can be reduced, in principle, by controlling the ion-exchange fabrication process that alters the refractive index distribution from the parabolic to an aspheric profile. However, all currently available commercial GRIN lenses possess nonaplanatic properties with noticeable spatial aberrations lying on and off the principle optical axis. The aberration of GRIN lenses can be compensated over a certain field of view and working distance by affixing additional optical elements, such as a plano-convex microlens [6]. However, the passive compensation approach requires specific design optimization for different GRIN endoscopes.

In this Letter, we propose the use of adaptive optics to correct the aberrations in GRIN endomicroscopy. Adaptive aberration correction using deformable mirrors has previously been used in optical microscopy for the correction of sample-induced aberrations [7,8]. Recently, the adaptive-optic aberration correction in two-photon endomicroscopy has been successfully demonstrated [9]. Here, we diagnose the aberrations in a GRIN probe and compare two distinct correction schemes based on the *preset* calibration and *in situ* feedback, respectively, in confocal GRIN endomicroscopy.

For experimental demonstration, we built an adaptive confocal laser-scanning microscope system [Fig. 1(a)] using a deformable mirror (DM). The DM (MIRAO-52, Imagine Optics Inc.) had 64 (8×8) individually controllable actuators with large strokes of +/ – 50 μm. The DM receives the excitation beam from a cw laser ($\lambda =$ 491 nm) at an angle of ~10°. The beam incident onto the DM was relayed onto two single axis galvanometer beam scanners (QS-10, Nutfield Tech). The DM and galvanometer mirrors lie in optical conjugate to the back pupil plane of a microscope objective lens (Model: LUCPLFLN 40×, NA = 0.6, Olympus Corp.). We use a Shack–Hartmann wavefront sensor (WFS, HASO, Imagine Optics Inc.) to verify that the confocal microscope setup, prior to the addition of the GRIN endoscope, was diffraction-limited. When no voltages were applied to the DM, the root mean square (RMS) wavefront error of the excitation beam at the focus of the objective lens was

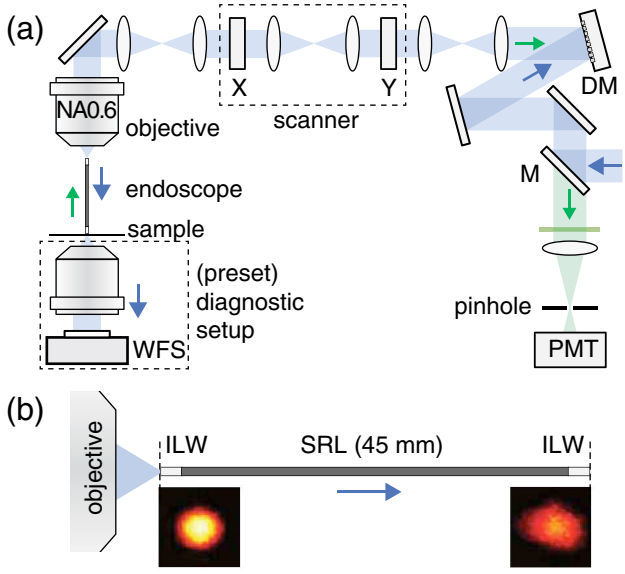

Fig. 1. (Color online) (a) Schematic of the experimental setup. DM, deformable mirror; M, dichroic mirror. (b) Beam profiles at the input and output of a triplet GRIN microendoscope.

0.14 μm, primarily due to the characteristic inhomogeneous membrane-actuator tension in the DM. When the DM was set to the flat-membrane state, the wavefront error was reduced to 0.031 μm. The DM was further adjusted to reduce the wavefront error to a minimum of 0.026 μm. This is the baseline setting before we begin to compensate for the aberration of the endoscope.

The endoscope was fabricated in-house using commercial GRIN lenses (Nippon Sheet Glass Co.). It had a triplet design, comprising of two imaging lenses (Model: ILW, NA = 0.45, 1/4 pitch) and a long relay lens (Model: SRL, NA = 0.1, 1 pitch). The probe measures 50 mm in length and 1 mm in diameter. The proximal surface of endoscope was placed at the focal plane of the objective lens. Figure 1(b) shows the typical beam profiles before and after the endoscope, as measured with a CCD camera. The beam distortion by the endoscope is evident. For optical characterization of the endoscope, a matching objective was placed after the endoscope to collimate the transmitted beam onto the Shack–Hartmann WFS. In confocal imaging, the back propagating fluorescent signal from a sample was collected via a descanned path, through a bandpass filter (519–541 nm) and focused with an achromatic lens through a pinhole (dia. = 50 μm, 2 Airy size) onto a photomultiplier tube.

We analyzed the on-axis aberrations of the GRIN endoscope. The transmitted wavefront measured with the WFS was decomposed to a set of orthogonal Zernike modes [7]: $\sum_{i=1}^{n} a_i Z_i(r,\phi)$, where a_i are the coefficients of the normalized Zernike polynomials $Z_i(r,\phi)$, where r is the normalized radial coordinates and ϕ is the azimuthal angle. Once the coefficients are determined, the DM is preset to arrange the excitation beam to have Zernike modes with opposite coefficients, so that a near diffraction-limited focus is formed after propagating through the endoscope. Fluorescence light generated at the focus was then collected by the endoscope. In the return path, the DM compensated the wavefront error induced in the fluorescence signal before entering the confocal pinhole.

We compared this preset scheme with an alternative approach where the optimal setting of the DM was found solely based on the appropriate metrics, such as sharpness and contrast, derived from the fluorescence image of a sample [7]. In this work, we used the Fourier-domain analysis of the images as the metric for image-based feedback [10]. Individual Zernike modes were sequentially introduced to the DM, and the coefficients that maximized the magnitudes of spatial frequencies were determined from a chosen fluorescence line profile. An iterative loop was used to find the optimal set of coefficients of the first 15 Zernike orders. Each loop takes around 10 iterations (frames).

Figure 2 shows the wavefront measurements of the beam at the WFS, when the DM was at the (a) baseline position, and adjusted with the (b) preset and (c) *in situ* optimized parameters, respectively. Before applying any compensation (a), the wavefront RMS error was about 0.64 μm. The Zernike analysis [Fig. 2(d)] shows significant tilt (Z_1 and Z_2) and defocusing (Z_3), which is related to the misalignment of the WFS with respect to the endoscope rather than the intrinsic aberration of the GRIN lenses. After removing these errors by adjusting the DM,

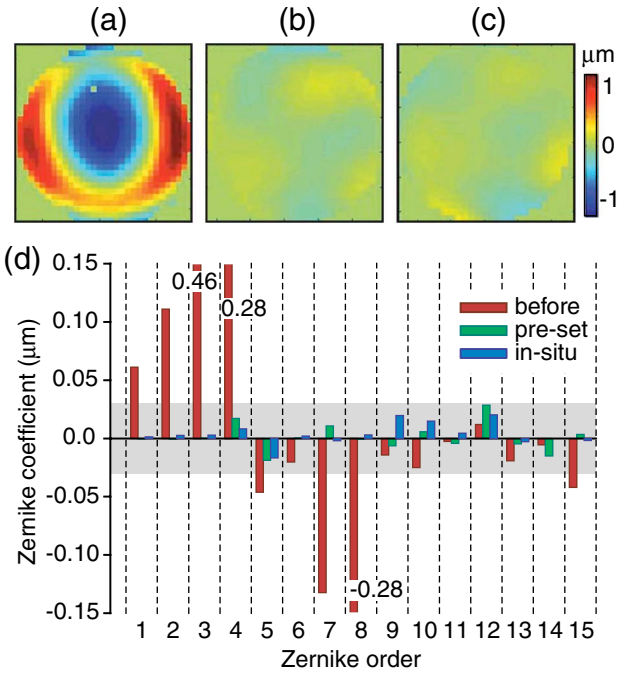

Fig. 2. (Color online) Measured wavefront distortion of GRIN endoscope (a) before correction, (b) with preset correction, and (c) with *in situ* correction. (d) The coefficients of the lowest 15 Zernike modes. Z_1 and Z_2, tip and tilt; Z_3, defocus; Z_4 and Z_5, astigmatism; Z_6 and Z_7, coma; Z_8, spherical aberration; Z_9 and Z_{10}, trefoil aberration.

the RMS error decreased to 0.42 μm. We found that most of the aberrations were confined to the lower Zernike orders, namely astigmatism (Z_4 and Z_5), coma (Z_6 and Z_7), and spherical aberration (Z_8). The relatively large astigmatism, $Z_4 = \sqrt{6}r^2\cos(2\phi)$, may be attributed to asymmetry in the refractive index distribution of the GRIN lenses. The outstanding spherical aberration, $Z_4 = \sqrt{5}(6r^4 + 6r^2 + 1)$, is typical of parabolic-profile GRIN lenses [11]. From this analysis and considering the finite number of actuators (8×8) in the DM, we used only the 10 lowest Zernike modes (Z_1 to Z_{10}) for correction. After correction, we found a significantly reduced wavefront RMS error of about 0.075 μm with both preset and 0.097 μm with *in situ* correction [Figs. 2(b) and 2(c)]. The Zernike coefficients measured after aberration corrections [Fig. 2(d)] were all less than 0.03 μm, i.e., $<0.06\lambda$. The residual wavefront error was higher than the baseline system performance of 0.026 μm, because of the residual uncompensated low and high-order aberrations [Fig. 2(d)].

We compared the performance of confocal imaging using a thin pine stem slide (301298, Carolina Scientific). Figure 3 shows the fluorescence images acquired with (a) only the tilt and field curvature removed and with (b) preset and (c) *in situ* adaptive compensation. The improvement in sharpness and contrast by aberration correction was evident over the entire field of view. Figure 3(d) shows representative line profiles of fluorescent signal along the same region in the sample.

GRIN lenses have relatively strong chromatic aberration, which manifests itself as a wavelength-dependent focal shift. In the case of single excitation wavelength, the chromatic aberration can be overcome simply by

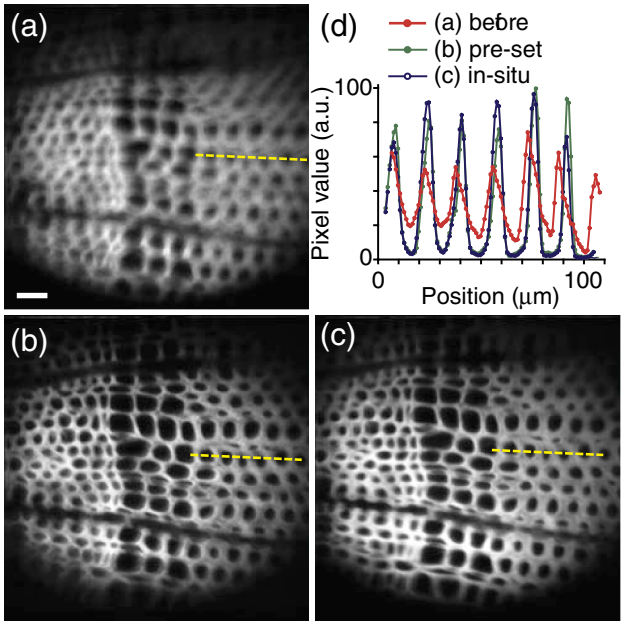

Fig. 3. (Color online) Fluorescence images of a pine stem specimen (a) before correction, (b) with preset correction, and (c) *in situ* correction. (d) Pixel values along the dotted lines in (a)–(c). Scale bar, 25 μm.

placing the pinhole at the confocal position optimized for the center wavelength of the emission band. The wavelength difference between the excitation and emission light was about 40 nm in this work, and it corresponds to a phase difference of 8% in the DM. This small phase offset does not significantly affect the aberration correction, as apparent in the results shown in Figs. 2 and 3.

The DM can be used to tune the focal position of the endoscope (by adjusting Z_3) up to tens of micrometers. This feature can be useful to correct for the chromatic focal shift in multicolor imaging using multiple excitation wavelengths. Furthermore, the remote focusing capability can facilitate three-dimensional imaging of biological tissues without having to move the endoscope and the sample.

In addition to the 50 mm long probe, we have also tested another triplet GRIN endoscope using a 1/2-pitch SRL relay lens (probe length: 28 mm) and obtained similar performance enhancements by aberration correction. Different applications may require different specifications for the probes in terms of the length, diameter, NA, working distance, or view angle. The adaptive-optic approach offers a flexible and effective solution that can accommodate a variety of GRIN endoscopes, each of which can be fabricated readily at low cost.

In principle, the *in situ* feedback approach has the advantage of correcting the wavefront distortions induced by the sample as well as by the endoscope. For thick-tissue imaging, we envision a hybrid scheme where the DM is first preset to compensate the endoscope aberration and is actively controlled to correct for the sample-dependent aberrations using an appropriate feedback algorithm. High-speed feedback methods have been developed for *in vivo* imaging [12,13].

In conclusion, we have successfully demonstrated the use of adaptive optics for the diagnosis and correction of aberration for GRIN confocal endomicroscopy. Both preset and *in situ* schemes were almost equally effective for compensating the aberrations of GRIN lenses, reducing the wavefront error by >4-fold (from 0.42 to <0.1 μm) and providing a substantial enhancement of the sharpness and contrast in confocal fluorescence images. We expect that the adaptive optics compensation may be extended to higher NA (e.g., 0.8) and also to multiphoton GRIN endoscopy. Instead of a deformable mirror, a spatial light modulator may be used for aberration correction with an advantage of substantially more tuning elements (e.g., 800 × 600) [14]. Adaptive-optic aberration correction is expected to facilitate *in vivo* imaging applications of GRIN endomicroscopy with the improvement of the image qualities.

We acknowledge the generous loan from P. Clemens with Imagine Optics, Inc., and thank J. Kim, M. Gather, and P. Kim for materials and discussions. This work is funded by the National Institutes of Health (NIH) (R21AI081010, RC1DK086242, RC2DK088661, U54CA143837, R01AI081734).

References

1. C. Liang, K. B. Sung, R. R. Richards-Kortum, and M. R. Descour, Appl. Opt. **41**, 4603 (2002).
2. P. Kim, E. Chung, H. Yamashita, K. E. Hung, A. Mizoguchi, R. Kucherlapati, D. Fukumura, R. K. Jain, and S. H. Yun, Nat. Methods **7**, 303 (2010).
3. R. P. J. Barretto, T. H. Ko, J. C. Jung, T. J. Wang, G. Capps, A. C. Waters, Y. Ziv, A. Attardo, L. Recht, and M. J. Schnitzer, Nat. Med. **17**, 223 (2011).
4. Z. G. Fan, J. Spencer, Y. Lu, C. Pitsillides, G. Singh, P. Kim, S. Yun, T. Strom, C. Lin, and M. Koulmanda, Nat. Med. **16**, 718 (2010).
5. D. T. Moore, Appl. Opt. **19**, 1035 (1980).
6. R. P. J. Barretto, B. Messerschmidt, and M. J. Schnitzer, Nat. Methods **6**, 511 (2009).
7. M. J. Booth, M. A. A. Neil, R. JuÅ¡kaitis, and T. Wilson, Proc. Natl. Acad. Sci. USA **99**, 5788 (2002).
8. A. Roorda, F. Romero-Borja, W. J. Donnelly, H. Queener, T. J. Hebert, and M. C. W. Campbell, Opt. Express **10**, 405 (2002).
9. F. Bortoletto, C. Bonoli, P. Panizzolo, C. D. Ciubotaru, and F. Mammano, PLoS ONE 6, e22321.
10. D. Debarre, M. J. Booth, and T. Wilson, Opt. Express **15**, 8176 (2007).
11. T. Sakamoto, Appl. Opt. **25**, 2613 (1986).
12. R. J. Zawadzki, S. S. Choi, A. R. Fuller, J. W. Evans, B. Hamann, and J. S. Werner, Opt. Express **17**, 4084 (2009).
13. N. Olivier, D. Débarre, and E. Beaurepaire, Opt. Lett. **34**, 3145 (2009).
14. A. J. Thompson, C. Paterson, M. A. A. Neil, C. Dunsby, and P. M. W. French, Opt. Lett. **36**, 1707 (2011).